Study of the Propagation Model for Large-Amplitude Internal Waves in Deep Sea

Jing Wang (王 晶)[1] Kai Guo (郭 凯)[1] and Junmin Meng (孟俊敏)[2*]

([1] *College of Information Science and Engineering, Ocean University of China, Qingdao, Shandong* 266100, *China*
[2] *First Institute of Oceanography, State Oceanic Administration, Qingdao, Shandong* 266061, *China*)

Abstract An amplitude of internal solitary wave as high as 100 m has been reported in the South China Sea(SCS). Large-amplitude internal waves may cause severe damage to the ocean engineering and submarine. The fully-nonlinear Schrödinger equation (FNLS) that describes large-amplitude internal-wave propagation in deep sea is derived from the governing equations of hydrodynamics by introducing the perturbation expansions with the assumption that the fluid is in a two-layer stratification system. This is a theoretical model for internal-wave dynamics, which is different from the well-known KdV series formula and BO equation. Moreover, a numerical simulation is carried out in the SCS. The results show that waveform and group velocity in evolution are in accordance with the MODIS images, so the model is suitable for simulating the large-amplitude internal-wave behavior in deep sea.

Key words oceanic optics; internal waves; fully-nonlinear Schrödinger equation; moderate resolution imaging spectroradiometer; numerical simulation

OCIS codes 280.4788

doi: 10.3788/CJL201239.s214004

1 Introduction

Internal waves are a kind of nonlinear wave motions in stratified fluids. Generally, they are generated by the tidal currents that encounter rough topography on the bottom of the ocean. The amplitude of internal waves ranges from less than 20 m to over 100 m. The large-amplitude internal waves, frequently generated in deep sea, can bring the transport of mass and momentum in a great level. At the same time, the global ocean circulation mainly occurs in deep water that is away from the continental shelf. So internal waves play important roles in maintaining the ocean circulation and global climate. In addition, the large-amplitude deep-sea internal waves are closely related to human activities such as marine engineering, shipping and military operations. The sea water will have strong inertia and stress force induced by the tremendous energy of internal waves in deep sea, which could cause adverse effects on the activities above.

The moderate-resolution imaging spectroradiometer (MODIS) sensor collects data in a continuous, systematic manner at 250-m resolution on a 2250-km swath[1]. It has almost worldwide coverage and could optically detect internal waves by the sunglint scattering. Because the sunglint scattering is greatly related to sea surface roughness, the surface convergence/divergence caused by internal waves may present dark/light bands in the MODIS images[2]. Based on this signature and high enough resolution, the MODIS is essential for internal wave optical detections and parametric inversion.

Many researchers intend to investigate the internal wave by establishing the theoretical model and carrying out numerical simulation for the wave propagation. As early as 1895, Korteweg and G. de Vries derived the KdV equation, which was a mathematical model of shallow-water waves with weakly nonlinear restoring forces. Until now, lots of studies on internal waves are based on this model[3]. Furthermore, Grimshaw [4] et al simulated the fully nonlinear internal wave propagation in shallow water by employing the EKdV equation. Benjamin and Ono[5] obtained the BO equation for describing internal waves in deep sea with a two-layer model approximation, and it requires wavelength be much larger than upper layer depth. Then, using mapping method, Peng et al[6] have obtained two kinds of soliton solutions to the nonlinear Schrödinger (NLS) equation. Chang et al[7] present a time-independent approach to compute the wave functions of NLS. More recently, our group proposed the weakly NLS in 2010[8], which was applicable to deep-sea internal waves with small amplitude compared to upper layer depth.

Our research is focused on the deep-sea internal waves with large amplitude. As a result, new theoreti-

收稿日期: 2012-08-03; **收到修改稿日期**: 2012-10-16

基金项目: 国家自然科学基金(61171161)资助课题。

作者简介: 王 晶(1962—),女,博士,教授,主要从事海洋内波和遥感测量等方面的研究。E-mail: wjing@ouc.edu.cn

* **通信联系人**。E-mail: mengjm@fio.org.cn

cal model needs to be constructed for demonstrating the internal wave behavior in systems with two layers. Besides, the bright/dark bands in optical MODIS images, which are generated by internal waves, will contribute to validate the result of numerous simulation.

2 Model description

In this paper, two-layer assumption is used: the upper layer with the density ρ_1, pressure p_1 and thickness h_1, the lower layer with the corresponding ρ_2, p_2, h_2 (Fig. 1). The continuity equation and Bernoulli equation in the upper layer is

$$\varphi_{xx}+\varphi_{zz}=0, \quad \zeta\leqslant z\leqslant h_1 \tag{1}$$

$$\varphi_t+\frac{1}{2}(\varphi_x^2+\varphi_z^2)+g\zeta=-\frac{p_1}{\rho_1}, \quad z=\zeta \tag{2}$$

where φ is the speed scalar potential, g is gravity acceleration and ζ is the displacement of interfacial pycnocline. From the upper rigid assumption, the kinematic boundary conditions are given by

$$\varphi_z=0. \quad z=h_1 \tag{3}$$

The boundary conditions at the interface are the continuity of normal velocity and pressure:

$$\zeta_t+\varphi_x\zeta_x=\varphi_z, \quad z=\zeta \tag{4}$$

$$p_1=p_2. \quad z=\zeta \tag{5}$$

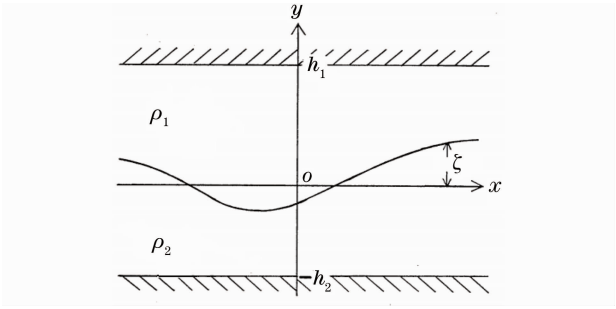

Fig. 1. Internal wave in two-layer configuration

Two dimensionless parameters are introduced[9]:

$$\varepsilon=\frac{A_0}{h_1}, \quad \mu=kh_1.$$

Here A_0 is maximum amplitude, and k is the wave number. Both ε and μ are considered as small parameters. More specifically, they require:

$$O(\varepsilon)=O(1), \quad \mu\ll 1.$$

Equation of weakly nonlinearity is based on $O(\varepsilon)=O(0)$. That is the key difference. The dimensionless forms of (1)～(4) are

$$\mu^2\varphi_{xx}+\varphi_{zz}=0, \quad \zeta\leqslant z\leqslant 1 \tag{6}$$

$$\mu^2(\varphi_t+\zeta)+\frac{1}{2}(\mu^2\varphi_x^2+\varphi_z^2)=-\mu^2 p_1, \quad z=\zeta \tag{7}$$

$$\varphi_z=0, \quad z=\zeta \tag{8}$$

$$\mu^2(\zeta_t+\varphi_x\zeta_x)=\varphi_z, \quad z=1 \tag{9}$$

Let $\varphi|_{z=1}=\varphi_0$. Substituting the Taylor expansions of φ and φ_z at $z=1$ into (7) and (9), it is obtained that

$$(\zeta-1)^2(-p_1)=-c_0^2\zeta(\zeta-1)+\zeta(\zeta-1)^2+\frac{1}{2}c_0^2\zeta^2. \tag{10}$$

(10) is dimensionalized as

$$\left(\frac{\zeta}{h_1}-1\right)^2\frac{-p_1}{\rho_1}=\left(g+\frac{c_0^2}{h_1}\right)\zeta+\left(\frac{k^2}{2}c_0^2-\frac{c_0^2}{2h_1}-\frac{2g}{h_1}\right)\zeta^2+\frac{g}{h_1^2}\zeta^3. \tag{11}$$

In the lower layer, the primitive governing equations become

$$\varphi_{xx}+\varphi_{zz}=0, \quad -h_2\leqslant z\leqslant\zeta \tag{12}$$

$$\varphi_t+\frac{1}{2}(\varphi_x^2+\varphi_z^2)=-g\zeta-\frac{p_2}{\rho_2}, \quad z=\zeta \tag{13}$$

$$\zeta_t+\varphi_x\zeta_x=\varphi_z, \quad z=\zeta \tag{14}$$

$$\varphi_z=0. \quad z=-h_2 \tag{15}$$

Substituting (11) into (13) yields

$$\left[\varphi_\tau+\frac{1}{2}(\varphi_x^2+\varphi_z^2)\right]\left[\left(\frac{\zeta}{h_1}-1\right)^2\right]=-c_1+c_2\zeta^2+c_3\zeta^3, \tag{16}$$

where c_1, c_2 and c_3 are listed as follows:

$$c_1=-\frac{(\rho_1-\rho_2)gh_1+\rho_1c_0^2}{\rho_2h_1}; \quad c_2=\frac{-\rho_1c_0^2+4(\rho_2-\rho_1)gh_1}{2\rho_2h_1^2}; \quad c_3=\frac{(\rho_1-\rho_2)g}{\rho_2h_1^2},$$

Differentiating (16) over t, x, z, three equations could be get. Combine them to one and seek series expansion of it in powers of ζ at $z=0$:

$$\left[\varphi_{tt}+\varphi_{ttz}\zeta+\frac{1}{2}\varphi_{ttzz}\zeta^2+(\varphi_x^2+\varphi_z^2)_t+(\varphi_x^2+\varphi_z^2)_{tz}\zeta+\frac{1}{2}\varphi_x(\varphi_x^2+\varphi_z^2)_x+\frac{1}{2}\varphi_z(\varphi_x^2+\varphi_z^2)_z\right]\times$$
$$\left[\left(\frac{\zeta}{h_1}-1\right)^2\right]+\left[\varphi_t+\varphi_{tz}\zeta+\frac{1}{2}(\varphi_x^2+\varphi_z^2)\right]\left[\frac{2}{h_1}\left(\frac{\zeta}{h_1}-1\right)(\varphi_z+\varphi_{zz}\zeta)\right]=$$
$$-c_1\varphi_z-c_1\varphi_{zz}\zeta-\frac{1}{2}c_1\varphi_{zzz}\zeta^2+2c_2\zeta\varphi_z+2c_2\zeta\varphi_{zz}\zeta+3c_3\zeta^2\varphi_z. \tag{17}$$

Similarly, the series expansion of (16) is:

$$-c_1\zeta=\left[\varphi_t+\varphi_{tz}\zeta+\frac{1}{2}\varphi_{tzz}\zeta^2+\frac{1}{2}(\varphi_x^2+\varphi_z^2)+\frac{1}{2}(\varphi_x^2+\varphi_z^2)_z\zeta\right]\left[\left(\frac{\zeta}{h_1}-1\right)^2\right]-c_2\zeta^2-c_3\zeta^3. \tag{18}$$

Now introduce two variables by the method of multiple scale: the spatial scales $x_0=x$, $x_1=\sigma x$, $x_2=\sigma^2x$ and the temporal scales $t_0=t$, $t_1=\sigma t$, $t_2=\sigma^2t$, where σ is a small parameter.

By the virtue of perturbation expansions, φ and ζ are shown as:

$$\varphi=\sum_{n=1}\sigma^n\varphi_n, \quad \zeta=\sum_{n=1}\sigma^n\zeta_n. \quad n=0,1,2,3,\cdots$$

Assume that the wave is evolving slowly, so φ_n is expanded further by

$$\varphi_n = \sum_n^{m=0} \varphi_{nm} \exp(\mathrm{i}m\psi) + \text{c. c.} \quad m = 0,1,2,3,\cdots.$$

Here m means the order of harmonic, and c. c. is the complex conjugate. Combining these expansions with (12), (15), (17) and (18), we compare the coefficients of the same exponent of e and get

$$\left(\frac{\partial^2}{\partial z^2} - m^2 k^2\right)\varphi_{nm} = F_{nm}, \quad -h_2 \leqslant z \leqslant \zeta \tag{19}$$

$$\left(c_1 \frac{\partial}{\partial z} - m^2 \omega^2\right)\varphi_{nm} = G_{nm}, \quad z = \zeta \tag{20}$$

$$\zeta_{nm} = -\frac{1}{c_1} H_{nm}, \quad z = \zeta \tag{21}$$

$$(\varphi_{nm})_z = 0. \quad z = -h_2 \tag{22}$$

By the solutions of above four equations and the use of recurrence relation about putting the results of last order ($n = j$) into the next order ($n = j + 1$), the Schrödinger equation can form its basic expressions.

When $n = 1$, let $\zeta_1 = \frac{1}{2}[A\exp(\mathrm{i}\psi) + \text{c. c.}]$, (19)~(22) will have the solution (23)~(25):

$$\varphi_1 = \varphi_{10} - \frac{c_1}{2\omega ch(kh_2)} ch[k(z+h_2)][\mathrm{i}A\exp(\mathrm{i}\psi) + \text{c. c.}], \tag{23}$$

$$\zeta_1 = \frac{1}{2}[A\exp(\mathrm{i}\varphi) + \text{c. c.}], \tag{24}$$

$$\omega^2 = c_1 kth(kh_2). \tag{25}$$

The φ_{10} and A, which are independent of z, are the functions in variables x_1, x_2, t_1, t_2, respectively.

From (25), the expression for c_g (group velocity) is found to be

$$c_g = \frac{\mathrm{d}\omega}{\mathrm{d}k} = \frac{\omega}{2k}\left[1 + \frac{2kh_2}{sh(2kh_2)}\right]. \tag{26}$$

When $n = 2$, equation (27)~(30) are obtained by solving (19)~(22) for second order:

$$\zeta_{20} = -\frac{1}{c_1}\varphi_{10t_1} + f_0 |A|^2, \tag{27}$$

$$A_{t_1} + c_g A_{x_1} = 0, \tag{28}$$

$$\varphi_{22} = f_1 ch[2k(z+h_2)]\mathrm{i}A^2, \tag{29}$$

$$\zeta_{22} = f_2 A^2, \tag{30}$$

When $n = 3$, let $\xi = x_1 - c_g t_1$, seeking the solution of (19)~(22) yields (31)~(33):

$$\varphi_{30} = -\frac{1}{2}\varphi_{10x_1x_1}(z^2 + 2h_2 z), \tag{31}$$

$$\varphi_{10\xi} = f_3 |A|^2 + s(\tau), \tag{32}$$

$$\varphi_{31} = \frac{\omega}{4ksh(kh_2)}\{z(z+2h_2)ch[k(z+h_2)]\mathrm{i}A_{x_1x_1} - 2(z+h_2)sh[k(z+h_2)]A_{x_2}\}, \tag{33}$$

In (32), $s(\tau)$ indicates a integration constant.

Substituting (32) into (20) gives

$$\mathrm{i}A_{t_2} + \mathrm{i}c_g A_{x_2} + \left[\frac{\omega h_2}{2kth(kh_2)} - \frac{c_g^2}{2\omega} - \frac{\omega^2 h_2}{c_1 k} c_g\right]A_{\xi\xi} + \left(\frac{f_3 f_6 c_g}{c_1} - \frac{f_7}{c_1} - k f_3\right)|A|^2 A + \gamma A = 0, \tag{34}$$

where γ also means the integration constant.

We define

$$\alpha = \frac{-\omega h_2}{2k\tan h(kh_2)} + \frac{c_g^2}{2\omega} + \frac{\omega^2 h_2}{c_1 k} c_g, \tag{35}$$

$$\beta = \frac{-f_6 f_3 c_g}{c_1} + \frac{f_7}{c_1} + k f_3, \tag{36}$$

the coefficients $f_0 \sim f_7$ are listed as follows:

$$f_0 = -\frac{1}{h_1} + \frac{\omega^2}{2c_1} - \frac{c_1 k^2}{4\omega^2}[1 + \tanh^2(kh_2)] + \frac{c_2}{2c_1},$$

$$f_1 = \left\{\frac{c_1\omega}{h_1} + \frac{c_1^2 k^2[2 + ch^2(kh_2)]}{4\omega ch^2(kh_2)} - \frac{c_2\omega}{2} - \frac{\omega^3}{4}\right\} \cdot [2c_1 ksh(2kh_2) - 4\omega^2 ch(2kh_2)]^{-1},$$

$$f_2 = -\left\{\frac{2\omega}{c_1} f_1 ch(2kh_2) + \left[\frac{1}{2h_1} + \frac{c_1 k^2}{8\omega^2 ch^2(kh_2)} - \frac{c_2}{4c_1} - \frac{\omega^2}{4c_1}\right]\right\},$$

$$f_3 = \frac{f_5 - c_g f_4}{c_g^2 - c_1 h_2}; \quad f_4 = -\frac{\omega^2}{4}\left[1 + \frac{1}{th^2(kh_2)}\right] - \frac{c_2}{2},$$

$$f_5 = \frac{\omega^3 h_2 th(kh_2)}{4} - \frac{\omega^3}{4k}\left[1 + \frac{kh_2}{th(kh_2)}\right] + \frac{c_1\omega}{2kh_1}\left[1 - \frac{\omega^2 h_2}{c_1} + \frac{kh_2}{th(kh_2)}\right] + \frac{c_1\omega}{2th(kh_2)} - \frac{c_2\omega}{2k}\left[1 + \frac{kh_2}{th(kh_2)}\right] + \frac{c_2\omega^3 h_2}{2c_1 k},$$

$$f_6 = \frac{\omega^3}{2c_1} - \frac{\omega}{h_1} - \frac{c_1 k^2}{2\omega} + \frac{c_2\omega}{c_1} - \frac{\omega}{h_2},$$

$$f_7 = \left(\frac{-c_1\omega}{h_1} + \frac{\omega^3}{2} + c_2\omega - \frac{c_1^2 k^2}{2\omega}\right)(f_2 - f_0) + \left(-\frac{4\omega^2}{h_1} + \frac{2\omega^2}{h_1} - 4c_1 k^2\right) f_1 ch(2kh_2) + \left(4k\omega^2 - \frac{2c_1 k}{h_1} + 2c_2 k\right) f_1 sh(2kh_2) - 2k^2 f_1 c_1[3sh^2(kh_2) + ch^2(kh_2)] - \frac{\omega^3}{2h_1 sh^2(kh_2)} - \frac{c_1^3 k^4}{8\omega^3 ch^2(kh_2)} + \frac{c_1^2 k^2}{8\omega h_1} + \frac{\omega^3}{8h_1} + \frac{c_1 k^2\omega}{2} - \frac{c_1 c_2 k^2}{4\omega} - \frac{3c_3\omega}{8} - \frac{3c_1\omega}{8h_1^2}.$$

Let $\xi_2 = x_2 - c_g t_2$, $t_2 = \tau$, in the new variables, (36) reads

$$-\mathrm{i}A_\tau + \alpha A_{\xi\xi} + \beta |A|^2 A + \gamma A = 0. \quad (37)$$

(37) is the deep-sea internal wave fully-nonlinear differential equation (FNLS). A stands for the amplitude, and α, β are defined as the dispersion coefficient and nonlinear coefficient, respectively. γ is the shoaling coefficient that depends on the gradient of bottom topography variation.

3 Numerical simulation for the FNLS

The equation derived in this paper is applicable to large-amplitude internal-waves propagation in deep sea. The aim of this section is to construct a numerical simulation for large-amplitude internal-wave propagation in actual SCS bathymetry conditions. After presenting the simulation results, the correctness of the model can be validated.

Large-amplitude internal waves are frequently observed primarily in the northern South China Sea (SCS) from Luzon Strait, and travel northwest to the continental shelf over the deep basin with the depth up to 3000 m. Our numerical simulation is based on the internal waves in the white rectangle region in Fig. 2(a). From the situ observation data in this area, the density is almost unchanged at the same depth. So we set the density of upper layer and lower layer as $\rho_1 = 1022.6\ \mathrm{kg/m^3}$ and $\rho_2 = 1025.5\ \mathrm{kg/m^3}$. The gravity acceleration is $g = 9.8\ \mathrm{m/s^2}$, and the depth of upper layer is $h_1 = 110$ m.

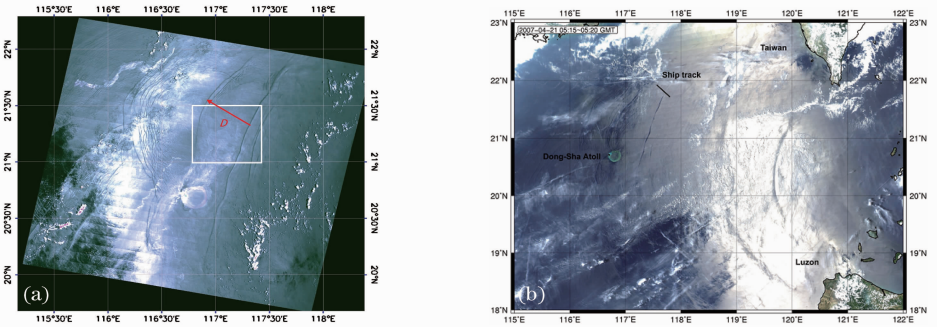

Fig. 2. Two MODIS images on SCS. (a) MODIS image acquired at 03:00 GMT on 5 July 2011; (b) MODIS image acquired at 05:20 GMT on 21 April 2007.

3.1 Simulation of internal-wave propagation

The numerical simulations are based on the FNLS equation (37). Here we use the split-step Fourier[10] method to provide the nonlinear equation a numerical solution, where the nonlinear and dispersion part could be treated separately with only a small error in a small

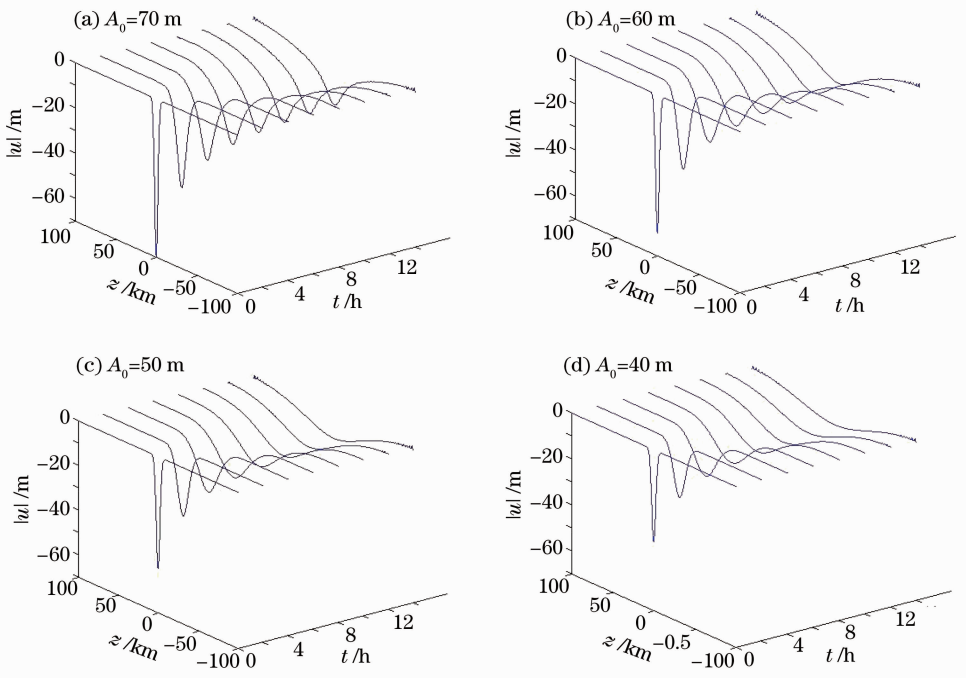

Fig. 3. Numerical evolution of waveform propagating from east to west in research region. (a) $A_0 = 70$ m; (b) $A_0 = 60$ m; (c) $A_0 = 50$ m; (d) $A_0 = 40$ m.

step. In this algorithm, it is important to choose the appropriate half width L and step size Δx, so that we could carry out an accurate and stable simulation. After repeating by N times, the wave with initial half width L will travel for a distance of $N\Delta x$. All the numerical simulations are performed on Matlab platform, where the waveform variation will be clearly displayed in the time-space evolution plot. Fig. 3 shows the numerical evolution simulations of a nonlinear-wave-packet propagating from west to east of research area. In Fig. 3, The t means propagation time, z means width of wave, and $|u|$ means the amplitude of internal wave. A_0 is initial amplitude.

Fig. 3 includes four different conditions where the initial amplitude A_0 is 70 m, 60 m, 50 m and 40 m, respectively. The initial waveform half-width L applied to all conditions is 2000 m and the step size $\Delta x = 1.32$ m. After traveling over 65 km, the internal-wave amplitude reduces to only 10 m, 12 m, 15 m and 22 m. Meanwhile, the width of four waveforms has been broadening all the time. We could conclude that the waveform, during propagation, tends to be more and more stable. Our simulation result does coincide with the remotely observed images in Fig. 2. The internal waves may cause the variation of ocean surface roughness, which optically displays dark and bright bands in satellite MODIS images. The distance between the dark and bright bands has a linear relation with the waveform width. In Fig. 2, we could find that the dark/bright distance is increasing when the wave travels from east to west. So this indicates that the numerical simulation is effective.

In order to understand why waveform broadens during propagation, a parametric study of α and β needs to be developed. We use the data of ρ_1, ρ_2, g and h_1 in former part of this section, and now α and β only depend on the lower layer depth h_2. By calculating (35) and (36), we have the distribution of α and β versus h_2 shown in Fig. 4(a) and Fig. 4(b), respectively.

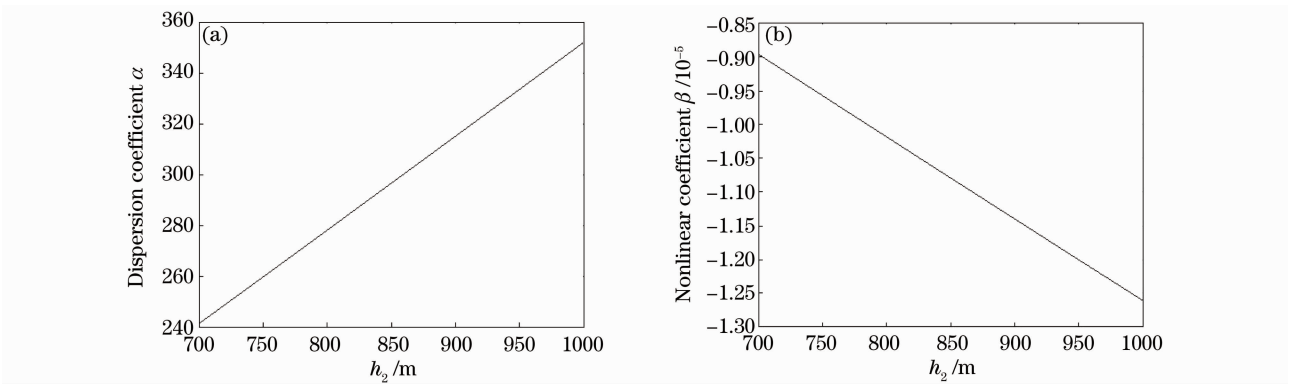

Fig. 4. Dispersion coefficient α and nonlinear coefficient β as a function of h_2 is shown in (a) and (b).

As the nonlinear internal waves will lose their energy over gradually sloping bathymetry, the value of α and β must be reducing in order to maintain the waveform. So Fig. 4 indicates the two effects described by our equation are coincident with rules of fact. (Note that the nonlinear coefficient β is in negative.) Besides, the nonlinear effect could make the waveform encounter breaking or distortion, while the dispersion effect tends to flat the waveform. According to Fig. 3, the internal wave tends to broaden as it propagations. The phenomenon implies it is the dispersion effect that gradually dominates in the interaction of the two effects and makes the waveform widen.

3.2 Group velocity verification

Another test for our theory is to calculate the group velocity c_g by (26) and gives the comparison with MODIS images. As many internal waves in SCS are generated by the semi-diurnal tides, their occurence cycle is about 12 hours. The adjacent waves indicated with red arrows in Fig. 2(a) are generated at the same source region but at different tidal cycles. Their separation is the distance of successive internal waves, which could be calculated by the longitude and latitude on the map. With the approximate distance D of 55 km in MODIS image and the tidal cycle T of 12 h, we estimate the velocity by $D/T = 1.28$ m/s. Meanwhile, the wave group speed obtained by (26) is $c_g = 1.32$ m/s . We could consider they are in good agreement because some external environmental parameters such as particular changes in stratification current and bathymetry are ignored here. So this may demonstrate that the FNLS model is accurate and suitable for large-amplitude internal-wave propagation in deep-sea.

4 Conclusions

In this paper, by using the method of perturbation expansions, we have derived the FNLS equation to describe the evolution of large-amplitude internal waves in two-layer deep water configurations.

Numerical simulations using the FNLS are performed in SCS by the step Fourier arithmetic on Matlab. The simulations demonstrate that the waveform tends to broaden and the amplitude gradually decreases. Compared with some MODIS images, the evolution plots and the theoretical group velocity are in agreement with the observed results. From further parametric study, we

find that the dispersion effect comes to dominate in the interaction with nonlinear effect and broadens the waveform during the wave′s propagation.

References

1 L. Mitnik, W. Alpers, K. S. Chen *et al*.. Manifestation of internal solitary waves on ERS SAR and SPOT images similarities and differences [C]. Proceedings of the 2000 International Geoscience and Remote Sensing Symposium (IGARSS′00), 2000, **5**: 1857～1859

2 C. Jackson. Internal wave detection using the moderate resolution imaging spectroradiometer (MODIS) [J]. *J. Geophysical Research*, 2007, **112**: C11012

3 Zhisong Fan, Yuanling Zhang, Mei Song. A study of SAR remote sensing of internal solitary waves in the north of the South China Sea: I. simulation of internal tide transformation [J]. *Acta Oceanologica Sinica*, 2008, **27**(4): 39～56

4 R. Grimshaw, E. Pelinovsky, T. Talipova. Solitary wave transformation in a medium with sigh-variable quadratic nonlinearity and cubic nonlinearity [J]. *Physica D: Nonlinear Phenomena*, 1999, **132**(1,2): 40～62

5 S. M. Sun. Solitary internal waves in continuously stratified fluids of great depth [J]. *Physica D: Nonlinear Phenomena*, 2002, **166**(1,6): 76～103

6 Peng Yanze, Shen Ming, Wang Zuojie. Exact solutions to the higher order nonlinear Schrödinger equation [J]. *Mathematica Applicata*, 2007, **20**(3): 505～511
彭彦泽，沈　明，王作杰. 高阶非线性薛定谔方程的精确解[J]. 应用数学, 2007, **20**(3): 505～511

7 S. L. Chang, C. S. Chien, B. W. Jeng. Computing wave functions of nonlinear Schrödinger equations: a time-independent approach [J]. *J. Computational Physics*, 2007, **226**(1): 104～130

8 Song Shiyan, Wang Jing, Meng Junmin *et al*.. Nonlinear Schrödinger equation for internal waves in deep sea [J]. *Acta Physica Sinica*, 2010, **59**(2): 1123～1129
宋诗艳，王　晶，孟俊敏 等. 深海内波非线性薛定谔方程的研究[J]. 物理学报, 2010, **59**(2): 1123～1129

9 R. Camassa, C. Viotti. A model for large-amplitude internal waves with finite-thickness pycnocline [J]. *Acta Appl. Math.*, 2012, **122**(1): 75～84

10 O. V. Sinkin, R. Holzlöhner, J. Zweck *et al*.. Optimization of the split-step Fourier method in modeling optical-fiber communications systems [J]. *J. Lightwave Technol.*, 2003, **21**(1): 61～68

栏目编辑：李文喆